

AFTERGLOWS AND MACRONOVAE ASSOCIATED WITH NEARBY LOW-LUMINOSITY SHORT-DURATION GAMMA-RAY BURSTS: APPLICATION TO GW170817/GRB170817A

DI XIAO^{1,2}, LIANG-DUAN LIU^{1,2}, ZI-GAO DAI^{1,2} AND XUE-FENG WU^{3,4}

¹School of Astronomy and Space Science, Nanjing University, Nanjing 210093, China; dxiao@nju.edu.cn, dzg@nju.edu.cn

²Key Laboratory of Modern Astronomy and Astrophysics (Nanjing University), Ministry of Education, China

³Purple Mountain Observatory, Chinese Academy of Sciences, Nanjing 210008, China and

⁴Joint Center for Particle, Nuclear Physics and Cosmology, Nanjing University-Purple Mountain Observatory, Nanjing 210008, China

Draft version April 23, 2019

ABSTRACT

A binary neutron star (BNS) merger has been widely argued to be one of the progenitors of a short gamma-ray burst (GRB). Such a central engine can be verified if its gravitational-wave (GW) event is detected simultaneously. Very recently, the association of GW170817 with short GRB170817A was reported by the LIGO/Virgo collaboration for the sake of excellent temporal and location coincidence. It is undoubtedly a landmark in multi-messenger astronomy and can greatly enhance our understanding of the BNS merger processes. Multi-wavelength follow-up observations have been carried out soon after the merger and X-ray, optical and radio counterparts have been detected, which are consistent with the predictions of the BNS merger scenario. Observationally, GRB170817A falls into the low-luminosity class which has a higher statistical occurrence rate and detection probability than the normal (high-luminosity) class. However, there is a possibility that GRB170817A is intrinsically powerful but we are off-axis and only observe its side emission. In this paper, we provide a timely modeling of the afterglow emission from this GRB and the associated macronova signal from the ejecta during a BNS merger, under the assumption of a structured jet, a two-component jet and an intrinsically low-energy quasi-isotropic fireball respectively. Comparing the properties of the afterglow emission with follow-up multi-wavelength observations, we can distinguish between the three models. Furthermore, a few model parameters (e.g., the ejecta mass and velocity) can be constrained.

Subject headings: gamma-ray burst: general – radiation mechanisms: non-thermal – gravitational waves

1. INTRODUCTION

Time domain astronomy has entered a new era since the monumental discovery of gravitational waves (GWs) by the advanced LIGO/Virgo observatories in the last two years (Abbott et al. 2016a,b, 2017a,b). Since then, searching for electromagnetic (EM) counterparts to GWs has become a very urgent issue in this field. Four convinced detections GW150914, GW151226, GW170104 and GW170814 are believed to originate from binary black hole (BBH) mergers with dozens of solar masses (Abbott et al. 2016a,b, 2017a,b). However, usually we would not expect any EM counterpart from BBH mergers except for several specific situations (Connaughton et al. 2016; Loeb 2016; Perna et al. 2016; Yamazaki et al. 2016; Zhang 2016; de Mink & King 2017). Differing with BBH mergers, the mergers of binary neutron stars (BNSs) are expected to generate a bunch of EM signals, such as short gamma-ray burst (GRB) jet emission (e.g. Faber et al. 2006; Nakar 2007; Giacomazzo et al. 2013; Berger 2014; Ruiz et al. 2016; Kathirgamaraju et al. 2017), cocoon prompt emission (Gottlieb et al. 2017; Lazzati et al. 2017a,b; Nakar & Piran 2017), jet/cocoon afterglow (e.g. Gottlieb et al. 2017; Lamb & Kobayashi 2017; Lazzati et al. 2017a; Nakar & Piran 2017), and macronova (Li & Paczyński 1998; Metzger et al. 2010; Metzger & Berger 2012; Kasen et al. 2013; Hotokezaka & Piran 2015; Gottlieb et al. 2017; Nakar & Piran 2017). Besides, a late-time (year-scaled) radio signal might originate from ejecta-medium

interactions as the ejecta enters the Sedov-Taylor phase (Nakar & Piran 2011).

Although BNS mergers have been proposed as one of the possible progenitors of short GRBs over three decades (Paczynski 1986; Eichler et al. 1989; Narayan et al. 1992; Mochkovitch et al. 1993) and there is a plenty of indirect evidence for such a scenario (e.g., for reviews see Nakar 2007; Berger 2014), a conclusive proof remains lacking. The detection of its GW emission will provide a unique way to verify this scenario once we can correlate a GW event with a short GRB. However, the advanced LIGO/Virgo GW detection horizon of BNS mergers is about one hundred of mega-parsec (Abadie et al. 2010; Martynov et al. 2016) and short GRBs rarely fall into this close range. Luckily, the first strong evidence of GW170817/GRB170817A association was found very recently (Abbott et al. 2017c), benefited from its relatively close distance. The host galaxy associated with this source is believed to be NGC 4993 that has a luminosity distance $D_L \simeq 40$ Mpc (Abbott et al. 2017d; Hjorth et al. 2017). Observationally, GRB170817A is rather weak (Connaughton et al. 2017; von Kienlin et al. 2017), with a duration $T_{90} \sim 2$ s and an isotropic luminosity $L_{\text{iso}} \sim$ a few $\times 10^{46}$ erg s⁻¹ (Goldstein et al. 2017; Zhang et al. 2017). According to the statistic analysis of the luminosity function and burst rate of short GRBs (Sun et al. 2015; Ghirlanda et al. 2016), nearby low-luminosity short GRBs (with luminosity e.g., $L_{\text{iso}} < 10^{48}$ erg s⁻¹) may be much more numerous than normal ones and we have a greater chance to detect them. Gener-

ally, the production of these low-luminosity short GRBs is assigned to less powerful central engines. Nevertheless, there is another possibility that we are off-axis and only observe the side emission of a normal short GRB. On one hand, even if the GW emission is detected for a BNS merger, we are very likely misaligned with the axis of the short GRB jet due to the finite small opening angle of a relativistic jet. In the standard picture, it is not easy for us to detect any off-axis EM signal because of the relativistic beaming effect. Alternatively, the side emission from an off-axis SGRB with a structured jet has been discussed as possible EM counterparts to GWs (Kathirgamaraju et al. 2017) and also several other radiation components besides the jet prompt emission have been proposed as possible counterparts in previous works (Gottlieb et al. 2017; Lamb & Kobayashi 2017; Lazzati et al. 2017a,b; Jin et al. 2017). On the other hand, the probability of observing the side emission is estimated to be much higher than the on-axis jet emission (Lazzati et al. 2017b). This kind of side emission should be much fainter than the jet from an observational point of view. Based on this argument, we consider several cases that the viewing angle θ_v varies. For large θ_v , it is possible that GRB170817A is intrinsically energetic. In this paper, therefore, we carry out calculations of multi-wavelength afterglow emission with different viewing angles under the assumption of a universally-structured jet and a two-component jet respectively, and then make a comparison with that of an intrinsically low-energy quasi-isotropic fireball. Our results show that such three types of model are distinguishable and can be tested by follow-up multi-wavelength observations. We apply these models to GRB170817A and find some parameters in the two-component jet model. Furthermore, we explore the macronova emission from a BNS merger for different ejecta parameters and compare it with the observations to obtain possible values of these parameters.

This paper is organized as follows. In Section 2 we introduce the universally-structured jet model and the two-component jet model, and calculate the off-axis afterglow emission. Then, we present the method of calculations for the macronova emission in Section 3. Section 4 shows our results for the two jet models and gives a comparison with an intrinsically low-energy quasi-isotropic fireball. Section 5 is an application to the very recently-discovered GW170817/GRB170817A. Lastly, we draw conclusions and provide a summary in Section 6.

2. OFF-AXIS AFTERGLOWS

In this section, we consider a structured jet with a lateral distribution of kinetic energy per solid angle $\varepsilon(\theta)$. This kind of jet may form during the propagation of the jet inside the ejecta, which gives rise to shocks at the jet head (Nagakura et al. 2014; Nakar & Piran 2017). The relativistic shocked jet material forms an inner cocoon, which is wrapped by an outer cocoon composed of mildly-relativistic shocked ejecta (Gottlieb et al. 2017; Nakar & Piran 2017; Lazzati et al. 2017a,b). Although there is some mixing between them, the cocoon is far from isotropy (Nakar & Piran 2017; Lazzati et al. 2017b). Thus, the overall uniform jet core plus structured cocoon system can be named as a structured jet, of which the kinetic energy per solid

angle and the initial Lorentz factor are assumed to be (Dai & Gou 2001; Zhang & Mészáros 2002a; Rossi et al. 2002; Kumar & Granot 2003)

$$\varepsilon(\theta) \equiv \frac{dE}{d\Omega} = \begin{cases} \varepsilon_0, & \text{if } \theta \leq \theta_c, \\ \varepsilon_0(\theta/\theta_c)^{-k}, & \text{if } \theta_c < \theta < \theta_m, \end{cases} \quad (1)$$

$$\Gamma_0(\theta) = \begin{cases} \Gamma_0, & \text{if } \theta \leq \theta_c, \\ \Gamma_0(\theta/\theta_c)^{-s}, & \text{if } \theta_c < \theta < \theta_m, \end{cases} \quad (2)$$

where the typical half opening angle of short GRBs $\theta_c \simeq 0.1$ (which is marginally consistent with the median opening angle given by Fong et al. 2015) and the maximum angle $\theta_m = 4\theta_c$ are assumed. The index k can be deduced from the luminosity distribution of local event rate density $\rho_0(> L)$. On one hand, the local event rate density of short GRBs can be fitted by a power-law $\rho_0(> L) \propto L^{-\lambda}$ with $\lambda \sim 0.7$ (Sun et al. 2015). Since $\rho_0(> L) \propto \Omega(> E) \simeq \pi\theta^2$ for similar durations of prompt emission, we can get $L \propto \theta^{-2/\lambda}$. On the other hand, the isotropic-equivalent luminosity $L \propto 4\pi \times dE/d\Omega \propto \theta^{-k}$. Therefore, $k = 2/\lambda \simeq 2.86$. In this paper, we adopt $k = 3$ as a nominal value. Generally the relationship of indexes s and k can be deduced from some empirical relations. Observationally, the relationship of initial Lorentz factor with isotropic equivalent energy approximates $\Gamma_0 \propto E_{\gamma, \text{iso}}^{1/4}$ (e.g. Zhang & Mészáros 2002b; Liang et al. 2010; Lü et al. 2012). Since $L \propto E_{\gamma, \text{iso}}$, we assume $s \simeq k/4$ in this work.

Similarly, a two-component jet can be described by the following angular distributions (e.g., Vlahakis et al. 2003; Huang et al. 2004; Lamb & Kobayashi 2017)

$$\varepsilon(\theta) = \begin{cases} \varepsilon_{\text{in}}, & \text{if } \theta \leq \theta_c, \\ \varepsilon_{\text{out}}, & \text{if } \theta_c < \theta < \theta_m, \end{cases} \quad (3)$$

$$\Gamma_0(\theta) = \begin{cases} \Gamma_{\text{in}}, & \text{if } \theta \leq \theta_c, \\ \Gamma_{\text{out}}, & \text{if } \theta_c < \theta < \theta_m, \end{cases} \quad (4)$$

where ε_{in} and ε_{out} and Γ_{in} and Γ_{out} represent the kinetic energies and Lorentz factors of the inner fast spine and outer slow sheath respectively.

For an off-axis viewing angle θ_v , the infinitesimal patch of the emission region at (r, θ, ϕ) makes an angle α with respect to the observer, which is given by (Kathirgamaraju et al. 2017)

$$\cos \alpha = \cos \theta_v \cos \theta + \sin \theta_v \sin \theta \cos \phi. \quad (5)$$

Assuming that the jet expands outward in a homogeneous medium with a typical number density $n \sim 10^{-2} \text{ cm}^{-3}$ for short GRBs (Fong et al. 2015), the evolution of the bulk Lorentz factor Γ can be obtained in the same way as previous works (e.g. Blandford & McKee 1976; Huang et al. 1999; Dai & Gou 2001). In this paper, we adopt the generic dynamics of a jet following Huang et al. (2000) without considering any lateral expansion of the jet. The radius and the time t' in the jet's comoving frame can be expressed by

$$\frac{dR}{dt} = \frac{c\beta}{1 - \beta \cos \alpha}, \quad (6)$$

and

$$\frac{dt'}{dt} = \frac{1}{\Gamma(1 - \beta \cos \alpha)}, \quad (7)$$

where $\beta \equiv (1 - 1/\Gamma^2)^{1/2}$.

Now we can calculate the synchrotron radiation of the electrons accelerated by the forward shock. Assuming the electrons have a power-law distribution $dn_e/d\gamma_e \propto \gamma_e^{-p}$, the minimum electron Lorentz factor is then $\gamma_m = [(p-2)/(p-1)]\epsilon_e(m_p/m_e)\Gamma$, where ϵ_e is a fraction of the post-shock energy density converted to electrons and the spectral index of the electron energy distribution $p = 2.5$ is adopted as a nominal value. The cooling Lorentz factor is $\gamma_c = 6\pi m_e c / (\sigma_T B'^2 t')$, where the magnetic field strength in the shocked medium is given by $B' = [32\pi\epsilon_B\Gamma(\Gamma-1)nm_p c^2]^{1/2}$ with ϵ_B being a fraction of the post-shock energy density converted to a magnetic field. In this paper, we adopt typical equipartition factors $\epsilon_e = 0.1$ and $\epsilon_B = 0.01$ for short GRBs (Fong et al. 2015). With these parameters, we can calculate the typical frequency ν'_m and the cooling frequency ν'_c . According to the relative values of the two frequencies, the spectrum without synchrotron self absorption (SSA) can be written (Sari et al. 1998). The SSA frequency ν'_a can be obtained by equating the blackbody luminosity at the Rayleigh-Jeans end with the synchrotron luminosity. At last, we can write down the complete differential luminosity $dL'_{\nu'}/d\Omega'$ in the jet's comoving frame (e.g. Dai & Gou 2001; Xiao & Dai 2017).

The observed total flux density of the off-axis afterglow is then given by (Dai & Gou 2001; Granot et al. 2002; Kathirgamaraju et al. 2017)

$$F_\nu = \int_0^{\theta_m} d\theta \int_0^{2\pi} d\phi \frac{dL'_{\nu'}/d\Omega'}{4\pi D_L^2 \Gamma^3 (1 - \beta \cos \alpha)^3}, \quad (8)$$

where D_L is the luminosity distance of the source to an observer. Similarly, the contribution of a counterjet can be accounted for if we integrate $d\theta$ from $\pi - \theta_m$ to π . The emission from the counterjet is insignificant at the beginning when Γ is large but could show up at later times as the jet decelerates to a non-relativistic speed. Note that we should integrate on the equal arrival time surface that is determined by $t = \int (1 - \beta \cos \alpha)/(c\beta) dR \equiv \text{constant}$ (Waxman 1997; Panaitescu & Mészáros 1998; Sari 1998; Huang et al. 2000; Moderski et al. 2000).

3. MACRONOVAE

The neutron-rich ejecta produced during a BNS merger undergoes rapid neutron capture (r -process) nucleosynthesis. The radioactive decay of these heavy nuclei is able to power a day-to-week-long macronova (also called kilonova) (Li & Paczyński 1998; Kulkarni 2005; Metzger et al. 2010; Kasen et al. 2013; Tanvir et al. 2013; Metzger 2017).

The density distribution of the ejecta can be obtained from numerical simulations. The geometry structure of the ejecta can be modeled as a partial sphere in the latitudinal and longitudinal direction (Kyutoku et al. 2013, 2015). We assume a homologous expansion inside the ejecta, so the density of the ejecta is (Kawaguchi et al. 2016)

$$\rho(v, t) = \frac{M_{\text{ej}}}{2\phi_{\text{ej}}\theta_{\text{ej}}(v_{\text{max}} - v_{\text{min}})} v^{-2} t^{-3}, \quad (9)$$

where v_{min} and v_{max} are the minimum and maximum velocities of the ejecta respectively, θ_{ej} is the polar opening angle, and ϕ_{ej} is the azimuthal opening angle. Here,

we adopt $v_{\text{min}} = 0.02c$, and $v_{\text{max}} = 2v_{\text{ej}} - v_{\text{min}}$. For a BNS merger, there exists a linearly correlation between θ_{ej} and ϕ_{ej} (Dietrich & Ujevic 2017),

$$\phi_{\text{ej}} = 4\theta_{\text{ej}} + \frac{\pi}{2}. \quad (10)$$

We assume that the macronova is powered by radioactive decay without an additional energetic engine such as a stable millisecond magnetar. The heating rate of r -process ejecta can be approximated by a power law (Korobkin et al. 2012; Tanaka 2016)

$$\dot{Q} \approx M_{\text{ej}}\epsilon_0 \left(\frac{t}{\text{day}}\right)^{-\alpha}, \quad (11)$$

where we adopt $\epsilon_0 = 1.58 \times 10^{10} \text{ erg s}^{-1} \text{ g}^{-1}$ and $\alpha = 1.3$ following Dietrich & Ujevic (2017).

The bolometric luminosity of macronova is approximated by (Kawaguchi et al. 2016; Dietrich & Ujevic 2017)

$$L_{\text{MN}} = (1 + \theta_{\text{ej}}) \dot{Q} \epsilon_{\text{th}} \times \begin{cases} t/t_c, & \text{if } t \leq t_c, \\ 1, & \text{if } t > t_c, \end{cases} \quad (12)$$

where the factor $(1 + \theta_{\text{ej}})$ indicates the contribution from radial edge effectively. ϵ_{th} is the thermalization efficiency introduced in Metzger et al. (2010), and we adopt $\epsilon_{\text{th}} = 0.5$ as a nominal value. The critical time t_c at which the expanding ejecta becomes optically thin (Kawaguchi et al. 2016) is

$$t_c = \left[\frac{\theta_{\text{ej}} \kappa M_{\text{ej}}}{2\phi_{\text{ej}}(v_{\text{max}} - v_{\text{min}})c} \right]^{1/2}. \quad (13)$$

For $t < t_c$, the mass of the photon-escaping region is $M_{\text{obs}}(t) = M_{\text{ej}}(t/t_c)$. At $t = t_c$, the whole region of the ejecta becomes transparent. Kasen et al. (2013) and Barnes & Kasen (2013) found that the opacity of r -process ejecta, particularly the lanthanides, is much higher than that for Fe-peak elements, with $\kappa \sim 10 - 100 \text{ cm}^2 \text{ g}^{-1}$. Kawaguchi et al. (2016) and Dietrich & Ujevic (2017) found that the bolometric light curve of the analytic model can well match the results of the radiation-transfer simulation performed in Tanaka & Hotokezaka (2013).

Assuming that the spectrum of macronova is approximated by a blackbody spectrum, the effective temperature can be written as

$$T_{\text{eff}} = \left(\frac{L_{\text{MN}}}{\sigma_{\text{SB}} S} \right)^{1/4}, \quad (14)$$

where σ_{SB} is the Stephan-Boltzmann constant and $S = R_{\text{ej}}^2 \phi_{\text{ej}}$ is the emitting area with $R_{\text{ej}} \simeq v_{\text{max}} t$ being the radius of the latitudinal edge. The observed flux at photon frequency ν can be calculated by

$$F_{\nu, \text{MN}} = \frac{2\pi h \nu^3}{c^2} \frac{1}{\exp(h\nu/k_B T_{\text{eff}}) - 1} \frac{R_{\text{ej}}^2}{D_L^2}, \quad (15)$$

where h is the Planck constant and k_B is the Boltzmann constant.

4. THEORETICAL RESULTS

Figure 1 shows our theoretical light curves of the structured jet model for different viewing angles. We consider a typical short GRB with jet core energy $\varepsilon_0 = 10^{50}$ erg/sterad and Lorentz factor $\Gamma_0 = 300$, located at a close distance $D_L = 40$ Mpc. With the increase of the viewing angle, the peak luminosity decays and the X-ray light curve shifts to earlier times until θ_v becomes larger than θ_m , which is different with previous works that assume $s = k$ (e.g. Moderski et al. 2000; Huang et al. 2000; Granot et al. 2002; Lamb & Kobayashi 2017). The reason for this is that the deceleration radius $R_{\text{dec}} \propto \varepsilon_0^{1/3} \Gamma_0^{-2/3}$ (e.g. Dai & Gou 2001), thus $R_{\text{dec}} \propto \theta^{-k/6}$ for the realistic $s = k/4$ case in this work, while $R_{\text{dec}} \propto \theta^{k/3}$ for the phenomenological $s = k$ case. For the parameters taken, the contributions from the counterjet (shown by the dashed lines in Figure 1(a)) are always negligible. The light curves of r-band are shown in Figure 1(b). Solid lines are corresponding to afterglow emission, and dashed and dotted lines to macronova emission. The theoretical flux of the macronova signal depends on the kinetic energy and velocity of the ejecta. Numerical simulations have suggested that the ejecta has typical mass $10^{-4} - 10^{-2} M_\odot$ and velocity $0.1 - 0.3c$ (e.g. Nagakura et al. 2014). Thus we consider two masses $10^{-3} M_\odot$ (magenta) and $10^{-2} M_\odot$ (red), and velocities $0.1c$ (dotted) and $0.3c$ (dashed), so we have four combinations. For large viewing angles, the macronova signal will probably dominate over the afterglow. Therefore, if the macronova component can be extracted in optical-infrared follow-up observations, it will help constrain parameters such as the viewing angle and the ejecta mass and velocity. For completeness, we plot the light curves of the radio band ($\nu = 5$ GHz) in Figure 1(c). Since the outer structured jet (including the cocoon) first sweeps up the ambient medium, the inner ejecta cannot catch up with the outer jet and thus the ejecta expands freely with a nearly constant velocity. Thus, we neglect any emission from the interaction of the ejecta with its ambient gas in a year-scale period after the merger (Nakar & Piran 2011). The time evolution of the afterglow spectrum is shown in Figure 1(d) for the $\theta_v = 4\theta_c$ case.

The theoretical results for the two-component jet model shown in Figure 2 are very different from those of the structured jet model. The line styles in this figure are the same with those in Figure 1. For an off-axis observer, the afterglow emission is dominated by the wide component at early times. The relevant parameters are $\Gamma_{\text{in}} = 300$, $\Gamma_{\text{out}} = 30$, $\varepsilon_{\text{in}} = 10^{50}$ erg/sterad and $\varepsilon_{\text{out}} = 10^{48}$ erg/sterad. The emission from the narrow component generally shows up later than 10^6 s. The ratio of peak luminosity between the wide and narrow component depends on the ratio of their energy and viewing angle. With the increase of θ_v , the peak time delays and the peak luminosity decays.

However, there is still a possibility that an observed low-luminosity burst is not due to the large viewing angle, instead, it arises from an intrinsically low-energy quasi-isotropic fireball. We need to consider its afterglow emission for completeness. The structured jet model can be easily generalized to an isotropic fireball case if we set index $k = 0$ and opening angle $\theta_m = \pi$ in Equation (1). Since the kinetic energy per solid angle along the line of sight in the structured jet model can be estimated by

$\varepsilon_0/\varepsilon_{\text{obs}} = (\theta_c/\theta_v)^{-k}$, to make a direct comparison with one of the previous cases (e.g., $\varepsilon_0 = 10^{50}$ erg/sterad, $\theta_v = 4\theta_c$), we assume a fireball with isotropic kinetic energy $E_{\text{iso}} \sim 4\pi \times 10^{50} \times 4^{-3} \text{ erg} \sim 2.0 \times 10^{49} \text{ erg}$. The corresponding X-ray, r-band, radio light curves and temporal evolution of the spectrum are shown in Figures 3. Different lines represent different medium densities, ranging from $n = 10^{-4} - 1 \text{ cm}^{-3}$. As is expected, the flux level drops with the decrease of n . We can clearly see that the observed afterglow emission of an intrinsically low-energy fireball is very different with that of an intrinsically powerful off-axis short GRB discussed above. The light curves rise and peak much earlier for the isotropic fireball model. In particular, comparing the yellow solid line in Figure 1(a) with the blue solid line in Figure 3(a), we can see that the peak time and peak luminosity differs (about one order of magnitude) for these two types of model. Similar differences can be found in r-band and radio band. Also, the quasi-isotropic macronova signal may be different since intrinsically-fainter short GRBs are likely accompanied by less energetic ejecta, so the macronova should be dimmer. The spectral evolution with time is also different from each other in the two types of model if we compare Figure 3(d) with Figure 1(d). All of these results would be testable by follow-up multi-wavelength observations.

5. APPLICATION TO GW170817/GRB170817A

In this section, we try to fit the multi-wavelength observational data (for a complete collection, see Abbott et al. 2017d) with the models above and the results are shown in Figure 4 and Figure 5. The X-ray upper limits are given by *Swift-XRT* and *NuSTAR* (Evans et al. 2017), while the two detections of *Chandra* are indicated by the red datapoints (Troja et al. 2017). For the optical band, we choose r-band to fit and the data are collected from various literatures (Andreoni et al. 2017; Arcavi et al. 2017; Pian et al. 2017; Smartt et al. 2017). The six radio datapoints ($\nu = 3$ GHz) are taken from Hallinan et al. (2017) and could give tight constraints on models. The quasi-isotropic fireball model is ruled out because the decaying light curve of it inevitably violates the early X-ray upper limits. The structured jet model can account for the *Chandra* X-ray data without violating the *Swift-XRT* and *NuSTAR* upper limits only if $\theta_v > \theta_m$. Obviously, the two-component model works well on X-ray emission. For the optical band, we use a Markov Chain Monte Carlo (MCMC) approach and the r-band data can be well fitted by a macronova component, while the afterglow emission is always sub-dominant, which is shown in Figure 4(b) and Figure 5(b). The MCMC best-fitting parameters for macronova component are $\tilde{M}_{\text{ej}} = 0.026 \pm 0.0016 (2\sigma)$ and $v_{\text{ej}} = (0.12 \pm 0.015)c (2\sigma)$, where $\tilde{M}_{\text{ej}} = (\kappa/10 \text{ cm}^2 \text{ g}^{-1}) \times (M_{\text{ej}}/M_\odot)$ is defined. The parameter corner is shown in Figure 6. The radio data can provide the tightest constraint on the models. The comparisons of the fitting results with radio observations are given in Figure 4(c) and Figure 5(c). Generally the two-component jet model gives the better-fitting quality than the structured jet model. However, the radio data are still dimmer than model predictions at all cases, indicating that there might be an extra component leading to the delayed X-ray emission (e.g. the contribution of a

reverse shock). Note that there are some degeneracies in parameters (energy, medium density, viewing angle, etc) and better-fitting quality can be achieved through fine tuning.

6. CONCLUSIONS

The discovery of multi-wavelength EM signals associated with GW170817 marks the beginning of a new era in multi-messenger time-domain astronomy. In this work we have re-investigated both an afterglow and a macronova which are associated with a nearby low-luminosity short GRB from a BNS merger, under the assumption of a universally structured jet and a two-component jet. Then we tried to apply the models to GRB170817A. Generally the isotropic fireball model is ruled out because it is fully inconsistent with the early X-ray upper limits and radio data. The structured jet model may explain the late-time X-ray emission but predict much more radio flux than observed. The multi-wavelength observational data could be well fitted by the two-component jet model and all the relevant parameters are within the reasonable range, although further fine tuning is needed.

Generally, detecting a low-luminosity short GRB is estimated to be much easier in our local universe than a normal one because the former has a much greater occurrence rate than the latter does. With the upgrade of the advanced LIGO/Virgo detectors and the improvement of the all sky transient survey, this kind of association will be more and more in the future. We have considered two possibilities that either a faint short GRB (like GRB170817A) is intrinsically low-luminosity and quasi-isotropic or it is just due to off-axis jet emission. We have shown that the properties of afterglow emission in these

cases are obviously different. The light curves rise slower and peak at a later time for the off-axis case. The spectrum is also different at any given time. Furthermore, if we assume the kinetic energy of the ejecta is proportional to that of the jet, the macronova signal in the low-energy fireball case should be much fainter than that of the off-axis powerful short GRB case. With follow-up multi-wavelength observations of a local low-luminosity short GRB, we can distinguish between these models very soon if such a kind of association is confirmed again in the future. In addition, several key parameters can be constrained such as the viewing angle, the ejecta mass, the ejecta velocity, and the ambient medium density, all of which would help reveal the mystery of short GRBs. For example, the ejecta parameters obtained in this paper are $(\kappa/10 \text{ cm}^2 \text{ g}^{-1}) \times (M_{\text{ej}}/M_{\odot}) = 0.026 \pm 0.0016$ (2σ) and $v_{\text{ej}} = (0.12 \pm 0.015)c$ (2σ) by considering the macronova component. These parameters are well consistent with numerical simulations of BNS mergers.

We thank Bing Zhang for useful discussions and constructive suggestions. This work was supported by the National Basic Research Program of China (973 Program grant 2014CB845800), the Strategic Priority Research Program “Multi-waveband gravitational wave Universe” (grant No. XDB23040000) of the Chinese Academy of Sciences, and the National Natural Science Foundation of China (grant No. 11573014, 11673068, and 11433009). XFW was also partially supported by the Youth Innovation Promotion Association (No. 2011231) and the Key Research Program of Frontier Sciences (QYZDB-SSW-SYS005).

REFERENCES

- Abadie, J., Abbott, B. P., Abbott, R., et al. 2010, *Classical and Quantum Gravity*, 27, 173001
- Abbott, B. P., Abbott, R., Abbott, T. D., et al. 2016a, *Phys. Rev. Lett.*, 116, 241103
- Abbott, B. P., Abbott, R., Abbott, T. D., et al. 2016b, *Phys. Rev. Lett.*, 116, 061102
- Abbott, B. P., Abbott, R., Abbott, T. D., et al. 2017a, *Phys. Rev. Lett.*, 118, 221101
- Abbott, B. P., Abbott, R., Abbott, T. D., et al. 2017b, *Phys. Rev. Lett.*, 119, 141101
- Abbott, B. P., Abbott, R., Abbott, T. D., et al. 2017c, *Phys. Rev. Lett.*, 119, 161101
- Abbott, B. P., Abbott, R., Abbott, T. D., et al. 2017d, *ApJL*, 848, L12
- Andreoni, L., Ackley, K., Cooke, J., et al. 2017, PASA, in press
- Arcavi, I., Hosseinzadeh, G., Howell, D., et al. 2017, *Nature*, DOI: 10.1038/nature24291.
- Barnes, J., & Kasen, D. 2013, *ApJ*, 775, 18
- Berger, E. 2014, *ARA&A*, 52, 43
- Blandford, R. D., & McKee, C. F. 1976, *Phys. Fluids*, 19, 1130
- Connaughton, V., Burns, E., Goldstein, A., et al. 2016, *ApJL*, 826, L6
- Connaughton, V., Blackburn, L., Briggs, M. S., et al. 2017, *GCN*, 21506
- Dai, Z. G., & Gou, L. J. 2001, *ApJ*, 552, 72
- de Mink, S. E., & King, A. 2017, *ApJL*, 839, L7
- Dietrich, T., & Ujevic, M. 2017, *Classical and Quantum Gravity*, 34, 105014
- Eichler, D., Livio, M., Piran, T., & Schramm, D. N. 1989, *Nature*, 340, 126
- Evans, P., Cenko, S., Kennea, J. A., et al. 2017, *Science*, doi:10.1126/science.aap9580
- Faber J. A., Baumgarte T. W., Shapiro S. L., Taniguchi K., 2006, *ApJL*, 641, L93
- Fong, W., Berger, E., Margutti, R., & Zauderer, B. A. 2015, *ApJ*, 815, 102
- Ghirlanda, G., Salafia, O. S., Pescalli, A., et al. 2016, *A&A*, 594, 84
- Giacomazzo B., Perna R., Rezzolla L., Troja E., Lazzati D., 2013, *ApJL*, 762, L18
- Goldstein, A., Veres, P., Burns, E. et al., 2017, *ApJL*, 848, L14
- Gottlieb, O., Nakar, E., & Piran, T. 2017, arXiv:1705.10797
- Granot, J., Panaitescu, A., Kumar, P., & Woosley, S. E. 2002, *ApJL*, 570, L61
- Hallinan, G., Corsi, A., Mooley, K. P., et al. 2017, *Science*, doi:10.1126/science.aap9855
- Hjorth, J., Levan, A. J., Tanvir, N. R. 2017, *ApJL*, 848, L31
- Hotokozaka, K., & Piran, T. 2015, *MNRAS*, 450, 1430
- Huang, Y. F., Dai, Z. G., & Lu, T. 1999, *MNRAS*, 309, 513
- Huang, Y. F., Gou, L. J., Dai, Z. G., & Lu, T. 2000, *ApJ*, 543, 90
- Huang, Y. F., Wu, X. F., Dai, Z. G., Ma, H. T., & Lu, T. 2004, *ApJ*, 605, 300
- Jin, Z. P., Li, X., Wang, H., et al. 2017, arXiv:1708.07008
- Kasen, D., Badnell, N. R., & Barnes, J. 2013, *ApJ*, 774, 25
- Kathirgamaraju, A., Duran, R. B., & Giannios, D. 2017, arXiv:1708.07488v1
- Kawaguchi, K., Kyutoku, K., Shibata, M., & Tanaka, M. 2016, *ApJ*, 825, 52
- Korobkin, O., Rosswog, S., Arcones, A., & Winteler, C. 2012, *MNRAS*, 426, 1940
- Kulkarni, S. R. 2005, arXiv:astro-ph/0510256
- Kumar, P., & Granot, J. 2003, *ApJ*, 591, 1075
- Kyutoku, K., Ioka, K., Okawa, H., Shibata, M., & Taniguchi, K. 2015, *Phys. Rev. D*, 92, 044028

- Kyutoku, K., Ioka, K., & Shibata, M. 2013, *Phys. Rev. D*, 88, 041503
- Lamb, G. P., & Kobayashi, S. 2017, arXiv:1706.03000v1
- Lazzati, D., Deich, A., Morsony, B. J., & Workman, J. C. 2017, *MNRAS*, 471, 1652
- Lazzati, D., López-Cámara, D., Cantiello, M., et al. 2017, arXiv:1709.01468v2
- Li, L. X., & Paczyński, B. 1998, *ApJL*, 507, L59
- Liang, E. W., Yi, S. X., Zhang, J., et al. 2010, *ApJ*, 725, 2209
- Loeb, A. 2016, *ApJL*, 819, L21
- Lü, J., Zou, Y. C., Lei, W. H., et al. 2012, *ApJ*, 751, 49
- Martynov, D. V., Hall, E. D., Abbott, B. P., et al. 2016, *Phys. Rev. D*, 93, 112004
- Metzger, B. D., Martínez-Pinedo, G., Darbha, S., et al. 2010, *MNRAS*, 406, 2650
- Metzger, B. D., & Berger, E. 2012, *ApJ*, 746, 48
- Metzger, B. D. 2017, *Living Reviews in Relativity*, 20, 3
- Mochkovitch, R., Hernanz, M., Isern, J., & Martin, X. 1993, *Nature*, 361, 236
- Moderski, R., Sikora, M., & Bulik, T. 2000, *ApJ*, 529, 151
- Nagakura, H., Hotokezaka, K., Sekiguchi, Y., Shibata, M., & Ioka, K. 2014, *ApJ*, 784, 28
- Nakar, E. 2007, *Phys. Rep.*, 442, 166
- Nakar, E., & Piran, T. 2011, *Nature*, 478, 82
- Nakar, E., & Piran, T. 2017, *ApJ*, 834, 28
- Narayan, R., Paczynski, B., & Piran, T. 1992, *ApJL*, 395, L83
- Panaitescu, A., & Mészáros, P. 1998, *ApJL*, 493, L31
- Paczynski, B. 1986, *ApJL*, 308, L43
- Perna, R., Lazzati, D., & Giacomazzo, B. 2016, *ApJL*, 821, L18
- Pian, E., D'Avanzo, P., Benetti, S., et al. 2017, *Nature*, DOI: 10.1038/nature24298
- Rossi, E., Lazzati, D., & Rees, M. J. 2002, *MNRAS*, 332, 945
- Ruiz M., Lang R. N., Paschalidis V., Shapiro S. L., 2016, *ApJL*, 824, L6
- Sari, R. 1998, *ApJL*, 494, L49
- Sari, R., Piran, T., Narayan, R. 1998, *ApJL*, 497, L17
- Smartt, S., Chen, T. W., Jerkstrand, A., et al. 2017, *Nature*, DOI: 10.1038/nature24303
- Sun, H., Zhang, B., & Li, Z. 2015, *ApJ*, 812, 33
- Tanaka, M., & Hotokezaka, K. 2013, *ApJ*, 775, 113
- Tanaka, M. 2016, *Advances in Astronomy*, 2016, 634197
- Tanvir, N. R., Levan, A. J., Fruchter, A. S., et al. 2013, *Nature*, 500, 547
- Troja, E., Piro, L., van Eerten, H. et al., 2017, *Nature*, DOI: 10.1038/nature24290
- von Kienlin, A., Meegan, C., & Goldstein, A. 2017, *GCNC*, 21520, 1
- Vlahakis, N., Peng, F., & Königl, A. 2003, *ApJL*, 594, L23
- Waxman, E. 1997, *ApJL*, 491, L49
- Xiao, D., & Dai, Z. G. 2017, *ApJ*, 846, 130
- Yamazaki, R., Asano, K., & Ohira, Y. 2016, *Progress of Theoretical and Experimental Physics A*, 19, 2385
- Zhang, B., & Mészáros, P. 2002a, *ApJ*, 571, 876
- Zhang, B., & Mészáros, P. 2002b, *ApJ*, 581, 1236
- Zhang, B. 2016, *ApJL*, 827, L31
- Zhang, B. B., Zhang, B., Sun, H. et al. 2017, *Nature Astronomy* submitted (arXiv: 1710.05851)

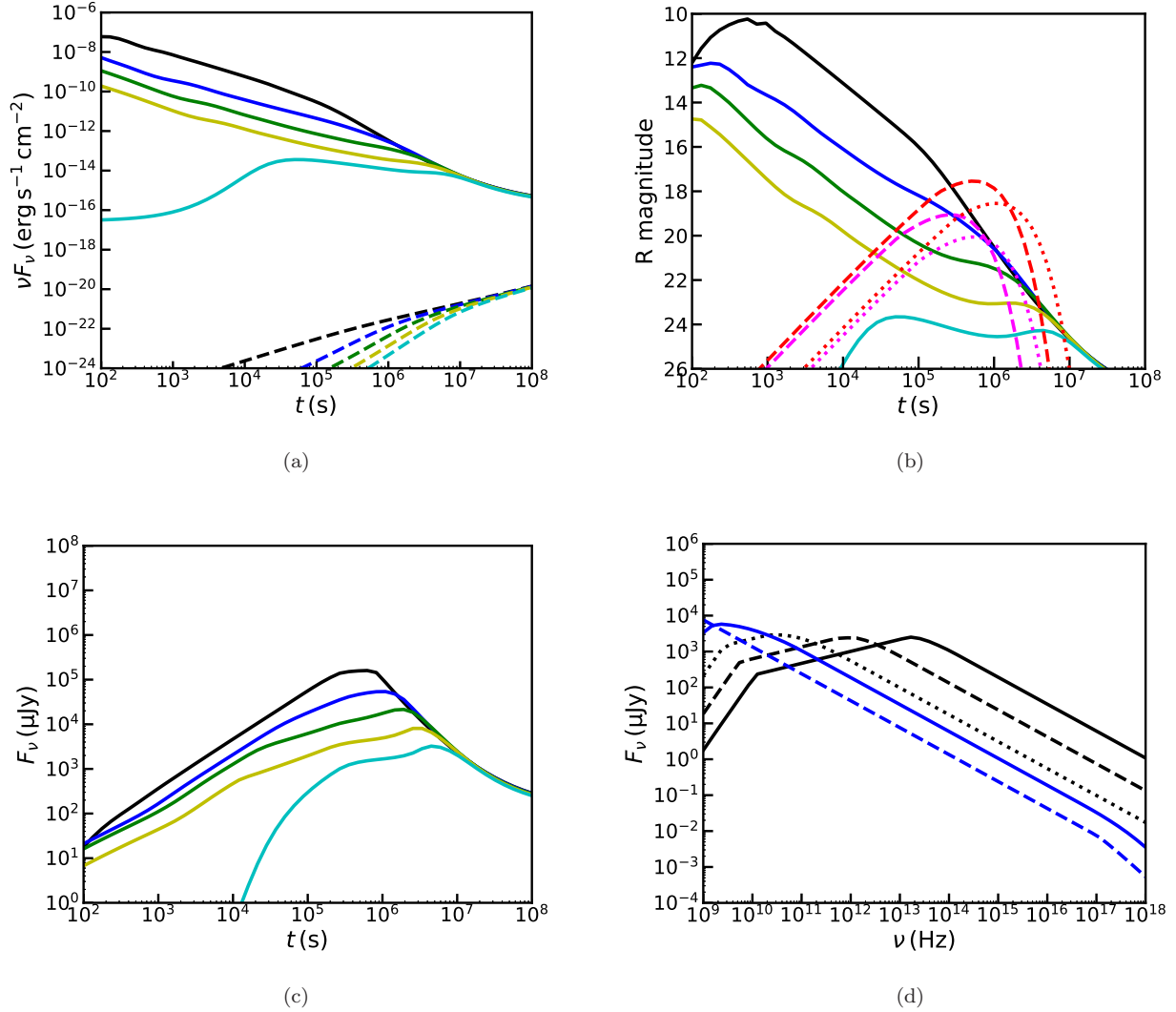


FIG. 1.— The theoretical results for the structured jet model. Panel (a): The X-ray light curves for different viewing angles. The black, blue, green, yellow and cyan solid lines are corresponding to $\theta_v = 0, 2\theta_c, 3\theta_c, 4\theta_c,$ and $5\theta_c$ respectively. The medium density is taken as $n = 10^{-2} \text{ cm}^{-3}$. The corresponding dashed line represent the contribution of a counterjet, which is at least three orders of magnitude fainter. Panel (b): The r-band magnitude for different viewing angles. The black, blue, green, yellow and cyan solid lines are corresponding to the afterglow emission of $\theta_v = 0, 2\theta_c, 3\theta_c, 4\theta_c,$ and $5\theta_c$ respectively. The four macronova signals for $\theta_{ej} = \pi/4$ can be distinguished by colors (magenta for $M_{ej} = 10^{-3} M_\odot$ and red for $M_{ej} = 10^{-2} M_\odot$) and line styles (dotted for $v_{ej} = 0.1c$ and dashed for $v_{ej} = 0.3c$). Panel (c): The radio ($\nu = 5$ GHz) light curves for different viewing angles. The line styles are the same as in panel (a). Panel (d): The spectrum evolution for the viewing angle $\theta_v = 4\theta_c$ case. The black solid, dashed, dotted, blue solid, and blue dashed lines represent the spectra at $t = 10^3, 10^4, 10^5, 10^6,$ and 10^7 s respectively.

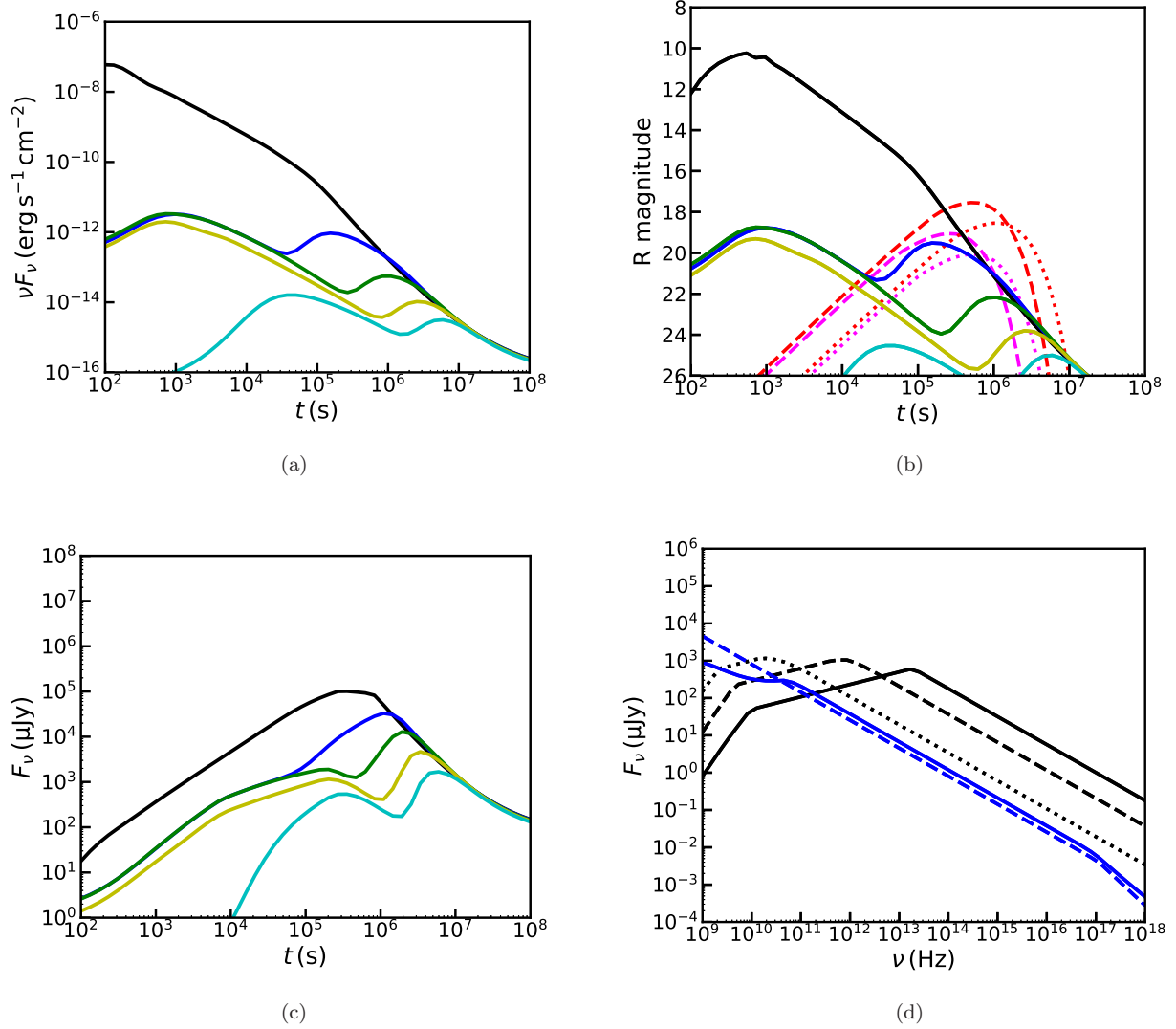


FIG. 2.— The theoretical results for the two-component jet model. Panel (a): The X-ray light curves for different viewing angles. The line styles are the same as in Figure 1(a). Panel (b): The r-band magnitude for different viewing angles. The line styles are the same as in Figure 1(b). Panel (c): The radio ($\nu = 5$ GHz) light curves for different viewing angles. The line styles are the same as in Figure 1(c). Panel (d): The spectrum evolution for the viewing angle $\theta_v = 4\theta_c$ case. The line styles are the same as in Figure 1(d).

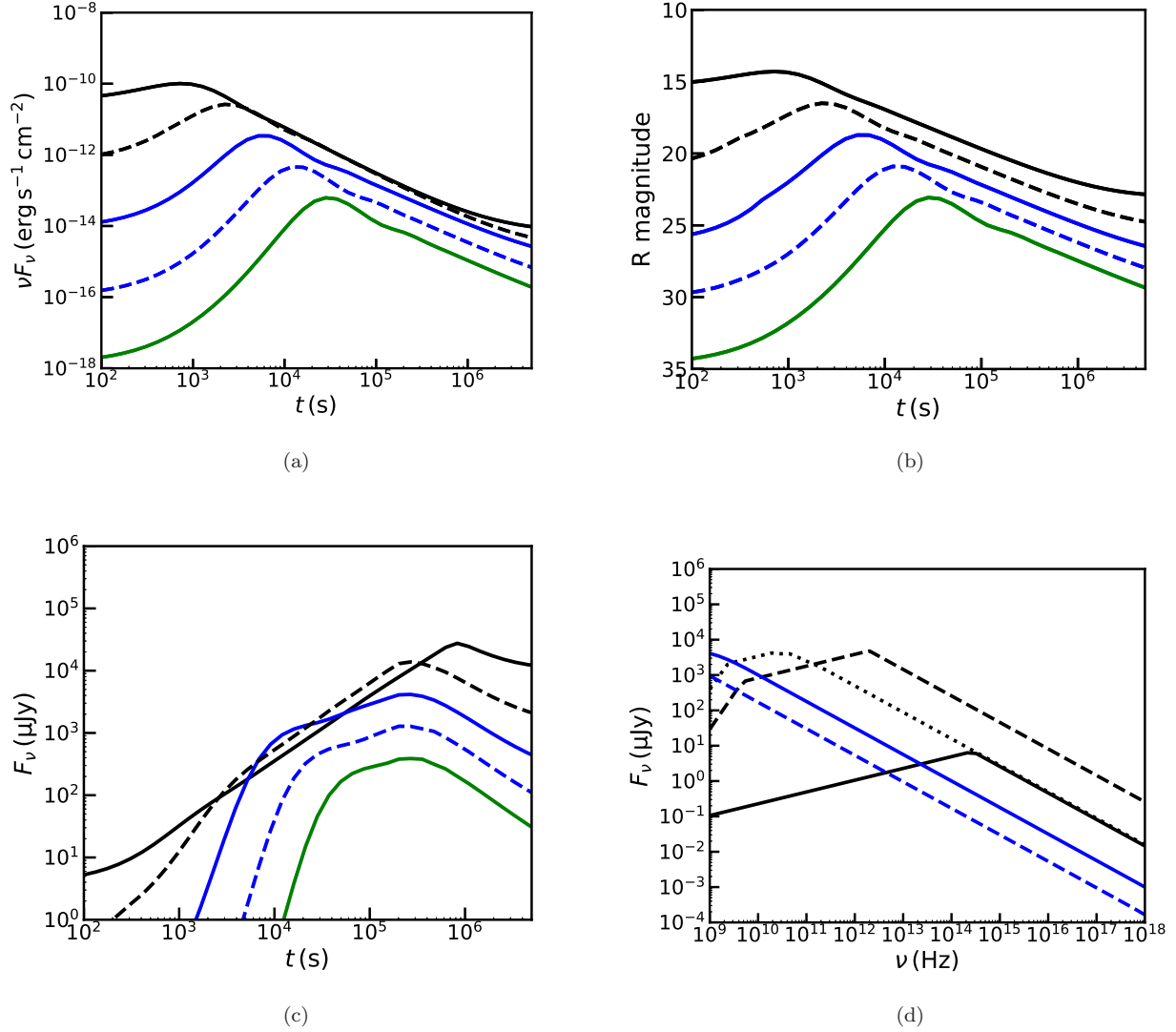


FIG. 3.— The theoretical results for the quasi-isotropic fireball model. Panel (a): The X-ray light curves for different medium densities. The black solid, dashed, blue solid, dashed and green solid lines represent $n = 1, 10^{-1}, 10^{-2}, 10^{-3}, 10^{-4} \text{ cm}^{-3}$ respectively. Panel (b): The r-band magnitude for different medium densities. The line styles are the same as in Figure 3(a). Panel (c): The radio ($\nu = 5 \text{ GHz}$) light curves for different medium densities. The line styles are the same as in Figure 3(a). Panel (d): The spectrum evolution for the viewing angle $\theta_v = 4\theta_c$ and $n = 0.01 \text{ cm}^{-3}$ case. The line styles are the same as in Figure 1(d).

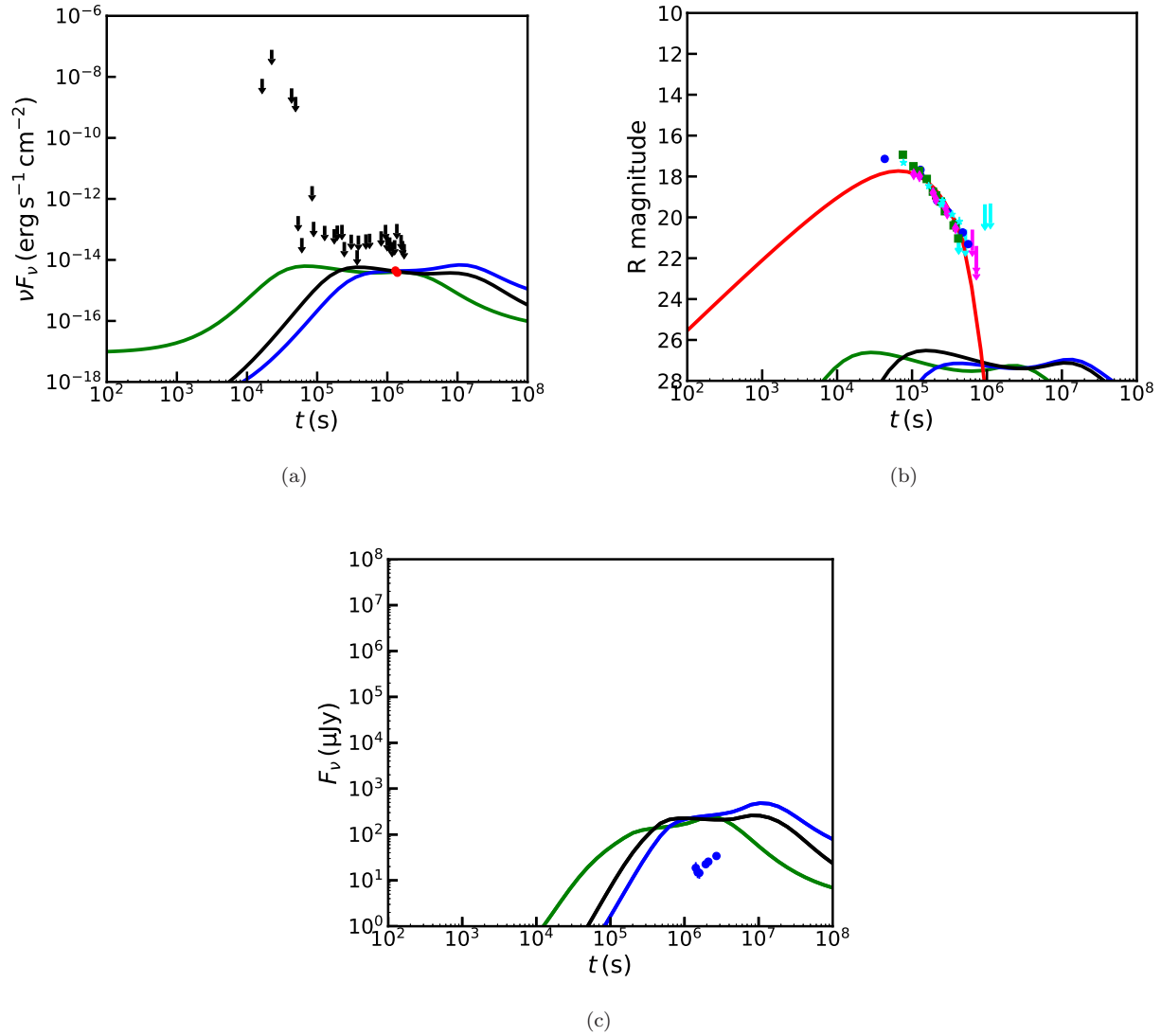


FIG. 4.— The fitting of multi-wavelength data with the structured jet model. Panel (a): The fitting of X-ray data (including black upper limits and red data-points) (Evans et al. 2017; Troja et al. 2017) with the structured jet model. Fitting parameters for different lines are shown in Table 1. Panel (b): The fitting of r-band data (blue datapoints-Pian et al. (2017); green datapoints-Arcavi et al. (2017); magenta datapoints and upper limits-Smartt et al. (2017); cyan datapoints and upper limits-Andreoni et al. (2017)) with the macronova emission plus the structured jet component. Panel (c): The comparison of the predicted flux with radio observations (blue datapoints) (Hallinan et al. 2017) for the structured jet model.

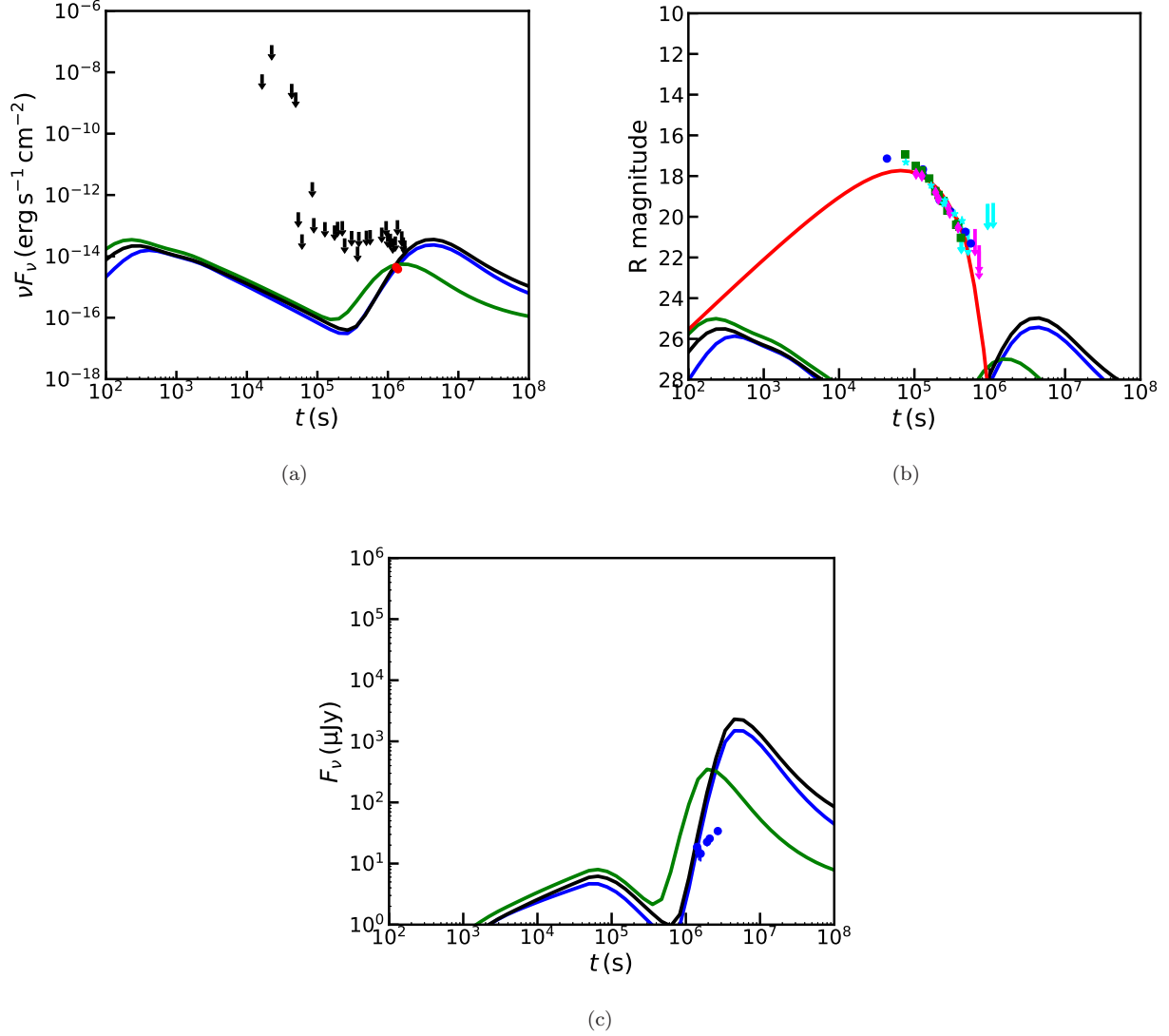


FIG. 5.— The fitting of multi-wavelength data with two-component jet model. Panel (a): The fitting of X-ray data (including black upper limits and red data-points) (Evans et al. 2017; Troja et al. 2017) with the two-component jet model. Fitting parameters for different lines are shown in Table 2. Panel (b): The fitting of r-band data (blue datapoints-Pian et al. (2017); green datapoints-Arcavi et al. (2017); magenta datapoints and upper limits-Smartt et al. (2017); cyan datapoints and upper limits-Andreoni et al. (2017)) with the macronova emission plus the two-component jet component. Panel (c): The comparison of the predicted flux with radio observations (blue datapoints) (Hallinan et al. 2017) for the two-component jet model.

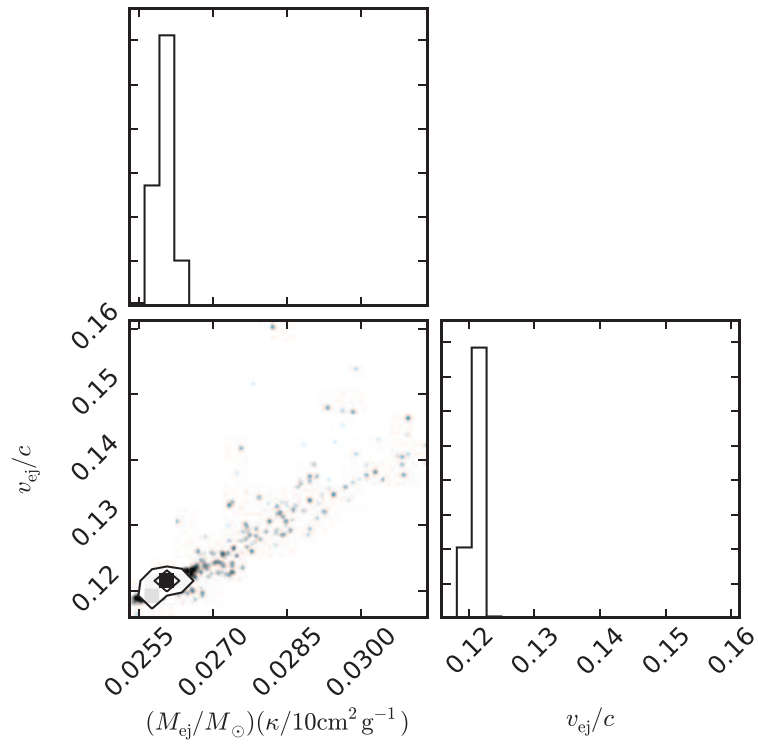


FIG. 6.— Parameter corner in modeling of r-band data. The contours are 1σ , 2σ , and 3σ uncertainties, respectively.

TABLE 1
FITTING PARAMETERS OF FIGURE 4.

	$\varepsilon_0(\text{erg/sterad})$	θ_v	$n(\text{cm}^{-3})$	Γ_0
Black line	10^{50}	$5\theta_c$	5×10^{-4}	300
Green line	10^{49}	$5\theta_c$	6×10^{-3}	300
Blue line	10^{50}	$5.5\theta_c$	10^{-3}	300

TABLE 2
FITTING PARAMETERS OF FIGURE 5.

	$\varepsilon_{\text{out}}(\text{erg/sterad})$	$\varepsilon_{\text{in}}(\text{erg/sterad})$	θ_v	$n(\text{cm}^{-3})$	Γ_{in}	Γ_{out}
Black line	10^{46}	10^{50}	$4\theta_c$	3×10^{-3}	300	30
Green line	10^{46}	10^{49}	$4\theta_c$	5×10^{-3}	300	30
Blue line	10^{46}	10^{50}	$3.6\theta_c$	10^{-3}	300	30